EXPERIMENTAL DEMONSTRATION OF E x B PLASMA DIVERTOR

by

E. J. Strait, D. W. Kerst and J. C. Sprott

May 1977

Plasma Studies PLP 722

University of Wisconsin

COO-2387-85

EXPERIMENTAL DEMONSTRATION OF $\vec{E} \times \vec{B}$ PLASMA DIVERTOR

by

E. J. Strait, D. W. Kerst, and J. C. Sprott

Department of Physics
University of Wisconsin-Madison
Madison, Wisconsin 53706 U.S.A.

The $\vec{E} \times \vec{B}$ drift due to an applied radial electric field in a tokamak with poloidal divertor can speed the flow of plasma out of the scrape-off region, and provides a means of externally controlling the flow rate and thus the width of the density fall-off. An experiment in the Wisconsin Levitated Toroidal Octupole, using $\vec{E} \times \vec{B}$ drifts alone, demonstrates divertor-like behavior, including 70% reduction of plasma density near the wall and 40% reduction of plasma flux to the wall, with no adverse effects on confinement of the main plasma.

In future generations of tokamaks it will become increasingly important to reduce the potentially large losses due to bremsstrahlung and line radiation by high-Z impurities. One method often proposed to isolate the plasma from the first wall of the containment vessel is the poloidal field divertor, and we suggest that externally applied $\vec{E} \times \vec{B}$ drifts could be used to speed the flow of plasma toward the divertor's pumping chamber.[1] This would provide external control of the flow velocity and thus of the width of the density fall-off (proportional to the square root of the transit time to the pumping chamber[2]), and could also remove some particles otherwise mirror-trapped in the divertor's "scrape-off" region. Somewhat similar ideas have been proposed by others.[3] The present experiment[4] is a first demonstration of this idea, using $\vec{E} \times \vec{B}$ drifts alone to produce divertor-like effects.

Figure 1 shows schematically the minor cross-section of a tokamak with a double-null poloidal field divertor, such as that proposed for the conceptual reactor UWMAK-III.[5] We have added to the picture segmented walls which are biased relative to the plasma, creating a radial electric field and thus an $\vec{E} \times \vec{B}$ drift into the divertor chambers as shown. The plasma is expected to shield out the electric field, causing it to be concentrated near the wall, just where it is desired most for this scheme, and this has been observed in other applied radial electric field experiments[6] as well as the present one. The existence of many inductively driven multipoles and tokamaks gives evidence for the ability of properly designed insulated gaps, such as the two "anti-divertor" gaps in Figure 1, to sustain a potential difference in the presence of plasma without disastrous arcing. Large plasma flux to the wall in the vicinity of the gap due to inductive electric fields on the falling half of the pulse, similar to the $\vec{E} \times \vec{B}$ drift out the divertor gap in Figure 1, has been predicted[7] and observed[8] in inductively driven multipoles.

In order for the $\vec{E} \times \vec{B}$ drift to make a significant contribution, the poloidal component of the $\vec{E} \times \vec{B}$ drift must be greater than that of the thermal flow along field lines: approximately $E > v_o B_p$ since $B_p << B_t$. Here B_p and B_t denote the poloidal and toroidal components respectively of the magnetic field, and v_o the flow velocity along field lines to the divertor (say, the ion acoustic speed, which equals ion thermal speed if $T_i \geq T_e$, as we will assume hereafter). Using B_p = 5 kG and considering ^{12}C impurities at 100 eV this gives E > 140 V/cm, a not unreasonable figure. The radial excursion of a single particle's guiding center from its unperturbed orbit due to the applied electric field, at the lower limit for E given above, is approximately $\rho B_p/B$, where ρ is the gyroradius. This is smaller than a gyroradius and much smaller than a banana width, hence even if the electric field penetrates past the divertor separatrix its effect on confined particles will be negligible.

An experiment has been carried out in the Wisconsin Levitated Toroidal Octupole[9] to demonstrate the use of $\vec{E} \times \vec{B}$ drifts to remove the outer edge of the plasma. Figure 2 is a minor cross-section of the octupole showing the poloidal field. A typical field strength is 2 kG in the region between the outer rings and the wall. The four current-carrying internal rings are inductively driven, and the field has a crowbarred decay time of > 70 ms. The rings can be levitated by temporarily withdrawing their supports during the field pulse, the supports remaining fully withdrawn for 20 ms. The plasma used was a hydrogen ECRH afterglow plasma, with peak density $\sim 5 \times 10^{10}$ cm^{-3}, $kT_e \sim 5$ eV, $kT_i < 1$ eV, and a decay time of about 15 ms.

A partial limiter, or fin, was installed on the upper lid, extending along a major radius, as shown in Figure 2. Note that it lies parallel to the field lines, unlike a conventional limiter. It can be biased relative to the wall, and can be

folded against the wall when not in use. Radial profiles of floating potential and ion saturation current are measured with a floating double probe between an outer ring and the wall. A probe mounted on a cart, movable toroidally and through a vertical arc at constant toroidal angle, is used to map floating potential and ion saturation current in ψ (poloidal flux function) and ϕ (toroidal angle). Plasma flux to the wall is measured with striped collectors.[10]

The upper outer ring is biased relative to the wall, in order to produce an $\vec{E} \times \vec{B}$ rotation of the plasma in the toroidal direction. Most of the potential drop appears near the wall in a layer about 2 cm $\approx$ 25 λ_D thick (see Figure 4(a)) and this is just where it is desired for this experiment. The fin is biased with the same sign as the ring, creating an $\vec{E} \times \vec{B}$ drift toward the wall on the side of the fin upstream relative to the main toroidal drift, and away from the wall on the other side. Thus a class of $\vec{E} \times \vec{B}$ drift surfaces are diverted toward the wall in the vicinity of the fin.

As V_{fin} is increased from 0, the location of the separatrix between diverted and undiverted drift surfaces moves deeper into the plasma, as observed by its influence on radial density profiles downstream, and saturates when $V_{fin} \gtrsim V_{ring}$. The flux of diverted plasma, measured by collectors on the fin and the wall near the fin, increases linearly with the $\vec{E} \times \vec{B}$ drift speed as V_{ring} (and proportionately V_{fin}) are increased, until saturating at V_{ring} = 40 V. At this bias the toroidal rotation period of the outer layer is about 1 ms, much shorter than the plasma lifetime but comparable to the time required for a particle to cross this layer and reach the wall. This corresponds to an $\vec{E} \times \vec{B}$ drift velocity of about 10^6 cm/s, of the same order as the ion acoustic velocity and much greater than the ∇B and curvature drifts.

Figure 3(a) shows experimentally measured drift surfaces for a particular pair of bias values in the saturated range of both. $\vec{E} \times \vec{B}$ drift surfaces are equivalent to surfaces of constant plasma potential, which are the same as surfaces of constant floating potential if $\nabla T_e = 0$, and the latter were measured with the cart probe. The 36.2 volt contour is the drift surface separatrix: drift surfaces outside this surface are diverted toward the wall, where one could imagine a divertor throat, although in this case the diverted plasma simply strikes the wall and is neutralized.

Ion saturation current (proportional to density if $\nabla T_e = 0$) was measured over the same range and is plotted in Figure 3(b) as the relative change from the case where the fin is retracted. There is little change on the upstream side except for a small increase as the denser plasma is diverted toward the wall, and there is a decrease of up to 70% on the downstream side, filling in farther downstream to a steady but reduced profile near the wall.

The corresponding radial profiles of floating potential and ion saturation current measured by the double probe at the outer wall, downstream by 15° or about 50 cm, are shown in Figure 4. The grounded fin as a mechanical obstacle has little effect on the density (ion saturation current) profile, but when the additional $\vec{E} \times \vec{B}$ drift toward the wall is present the density near the wall is greatly reduced and the scale length is approximately halved. The profile near the density peak, including the octupole separatrix where the majority of the particles are confined, shows no change with the insertion of the biased fin. Full I-V characteristics for the probe show that T_e is unchanged by the presence of the biased fin, even on a diverted drift surface, so the decrease in ion saturation current near the wall is indeed due to a decrease in density. The floating potential profiles for the three cases are indistinguishable.

Figure 4 also shows the same profiles for the case of an added weak toroidal field ($\sim$ 400 G at the minor axis). Evidently parallel resistivity is large enough to prevent the biased fin from charging entire flux surfaces, as the behavior is quite similar to the case with poloidal field only.

Although the divertor region is quite localized in ϕ, its influence on wall flux extends all the way around the machine. Figure 3(c) shows the wall flux measured by the striped collectors up to 360° downstream from the fin, plotted in terms of the relative change from the case with the fin retracted. There is an increase just upstream of the fin, a sharp decrease immediately downstream, and a general reduction by 30 to 40% all around the toroid.

This experiment, using $\vec{E} \times \vec{B}$ drifts alone, shows behavior desired of a divertor: a decrease in density near the wall with no deleterious effects on confinement of the dense central plasma, and reduction of plasma flux to the wall everywhere away from the divertor region. These effects were not seen when either the fin was grounded or the ring was not biased; this shows that they were due to the $\vec{E} \times \vec{B}$ drifts and not simply to the presence of the fin as a mechanical obstacle.

In the future we plan to add a poloidal magnetic field divertor to the octupole and use larger ratios of B_t/B_p, in order to more closely simulate a tokamak. This divertor will be capable of operating alone or with an $\vec{E} \times \vec{B}$ drift into the divertor throat, for purposes of comparison.

We are grateful for the assistance of P. D. Nonn in the construction of the retractable fin. The work was sponsored by U.S. E.R.D.A.

REFERENCES

1. D. W. Kerst, Bull. Am. Phys. Soc. 20, 1334 (1975).
2. According to simple divertor models: see, for example, D. M. Meade, et al., in Plasma Physics and Controlled Nuclear Fusion, Proc. 5th Int. Conf., Tokyo, 1974 (IAEA, Vienna, 1975), Vol. I, p. 605.
3. S. I. Braginskii, Sov. J. Plasma Physics 1, 202 (1975); T. Consoli, et al., in Plasma Physics and Controlled Nuclear Fusion, Proc. 5th Int. Conf., Tokyo, 1974 (IAEA, Vienna, 1975), Vol. I, p. 571; B. Lehnert, Nuclear Fusion 11, 485 (1971).
4. E. J. Strait and J. C. Sprott, Bull. Am. Phys. Soc. 21, 1062 (1976).
5. R. W. Conn et al., in Plasma Physics and Controlled Nuclear Fusion, Proc. 6th Int. Conf., Berchtesgaden, 1976 (IAEA, Vienna, 1977), Vol. III, p. 203.
6. M. Okabayashi and S. Yoshikawa, Phys. Rev. Lett. 29, 1725 (1972); J. R. Roth and G. A. Gerdin, "Characteristics of the NASA Lewis Bumpy-Torus Plasma Generated with High Positive or Negative Potentials," NASA TN D-8211 (1976).
7. K. Evans, Phys. Fluids 16, 2330 (1973).
8. A. J. Cavallo, Ph.D. thesis, Physics Dept., University of Wisconsin, Madison, Wis. (1975), p. 94.
9. H. K. Forsen, D. W. Kerst, R. A. Breun, A. J. Cavallo, J. R. Drake and J. C. Sprott, Proc. 4th Eur. Conf. on Controlled Fusion and Plasma Physics, Rome, 1970, p. 24.
10. E. R. Mosburg, J. Appl. Phys. 40, 5290 (1969); D. E. Lencioni and D. W. Kerst, Bull. Am. Phys. Soc. 15, 1466 (1970); A. J. Cavallo, Phys. Fluids 19, 394 (1976).

FIGURE CAPTIONS

Fig. 1. Minor cross-section of tokamak with double-poloidal-null divertor. Radial electric field (arrows) applied by biased wall segments results in $\vec{E} \times \vec{B}_t$ drift (double arrows) toward pumping chamber.

Fig. 2. Minor cross-section (with poloidal flux lines) of Wisconsin Levitated Octupole, showing locations of retractable fin and diagnostics (not all at same toroidal position). ψ_{sep} is octupole separatrix, ψ_{crit} is last MHD stable field line (minimum of $\oint dl/B$).

Fig. 3. Experimentally measured quantities plotted vs. ϕ (toroidal angle). $V_{ring} = 40$ V, $V_{fin} = 60$ V, B_p only. (a) and (b) are contour plots in ψ (poloidal flux function) and ϕ. Distance from minor axis along mid-cylinder is also shown. (a) Floating potential contours at 2-volt intervals. Arrowheads show direction of resulting $\vec{E} \times \vec{B}$ drift. Dotted line (36.2 volt contour) is drift separatrix. (b) Contours of relative change in density. (c) Relative change in wall flux. Vertical dotted lines show range in ϕ of Figs. 3(a) and (b).

Fig. 4. Radial profiles of (a) floating potential and (b) ion saturation current, 15° downstream from fin. $V_{ring} = 40$ V. Location of drift separatrix is taken from Fig. 3(a).

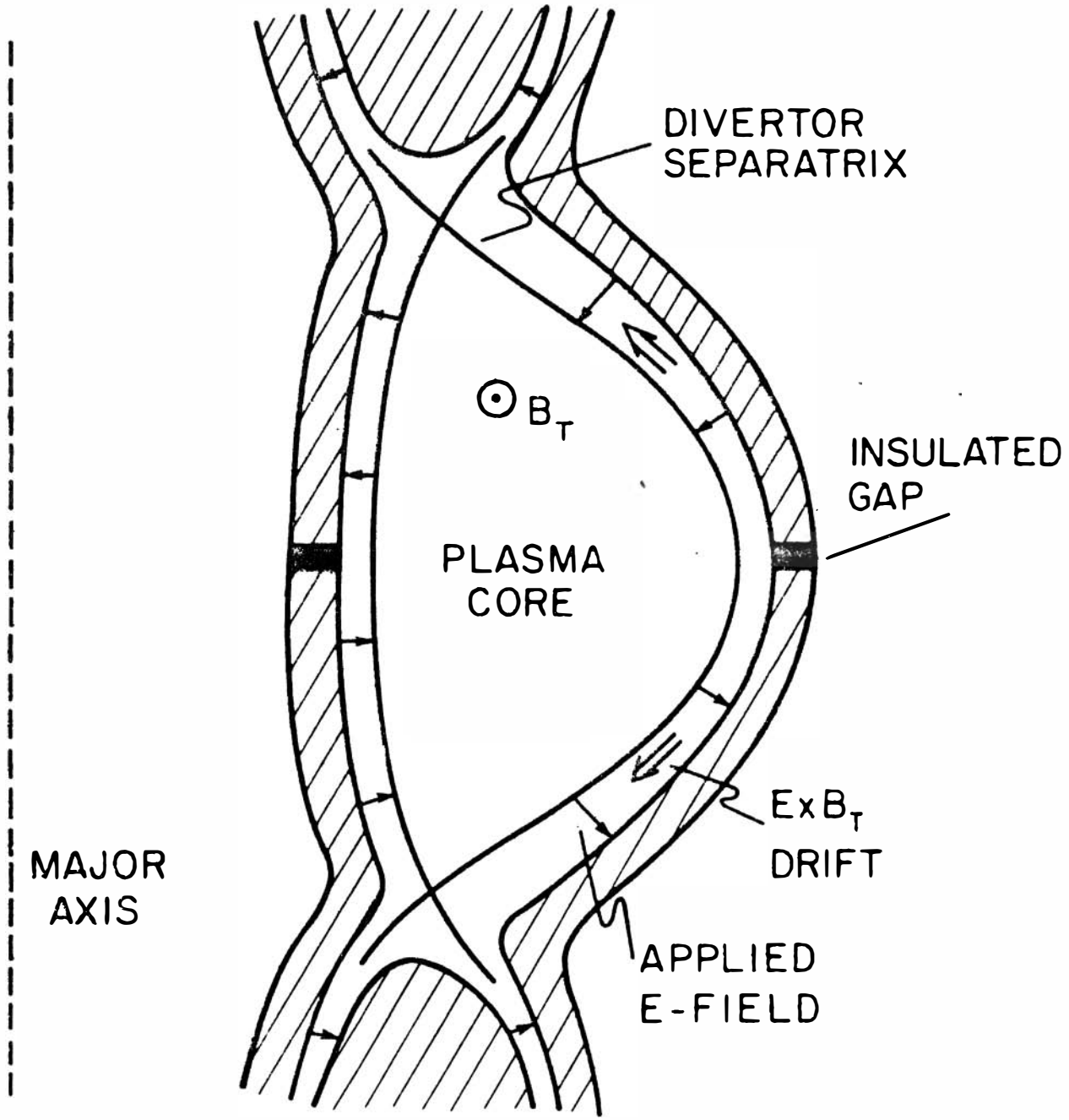
DIVERTOR
SEPARATRIX
B_T
INSULATED
GAP
PLASMA
CORE
$E \times B_T$
DRIFT
MAJOR
AXIS
APPLIED
E-FIELD

Figure 1

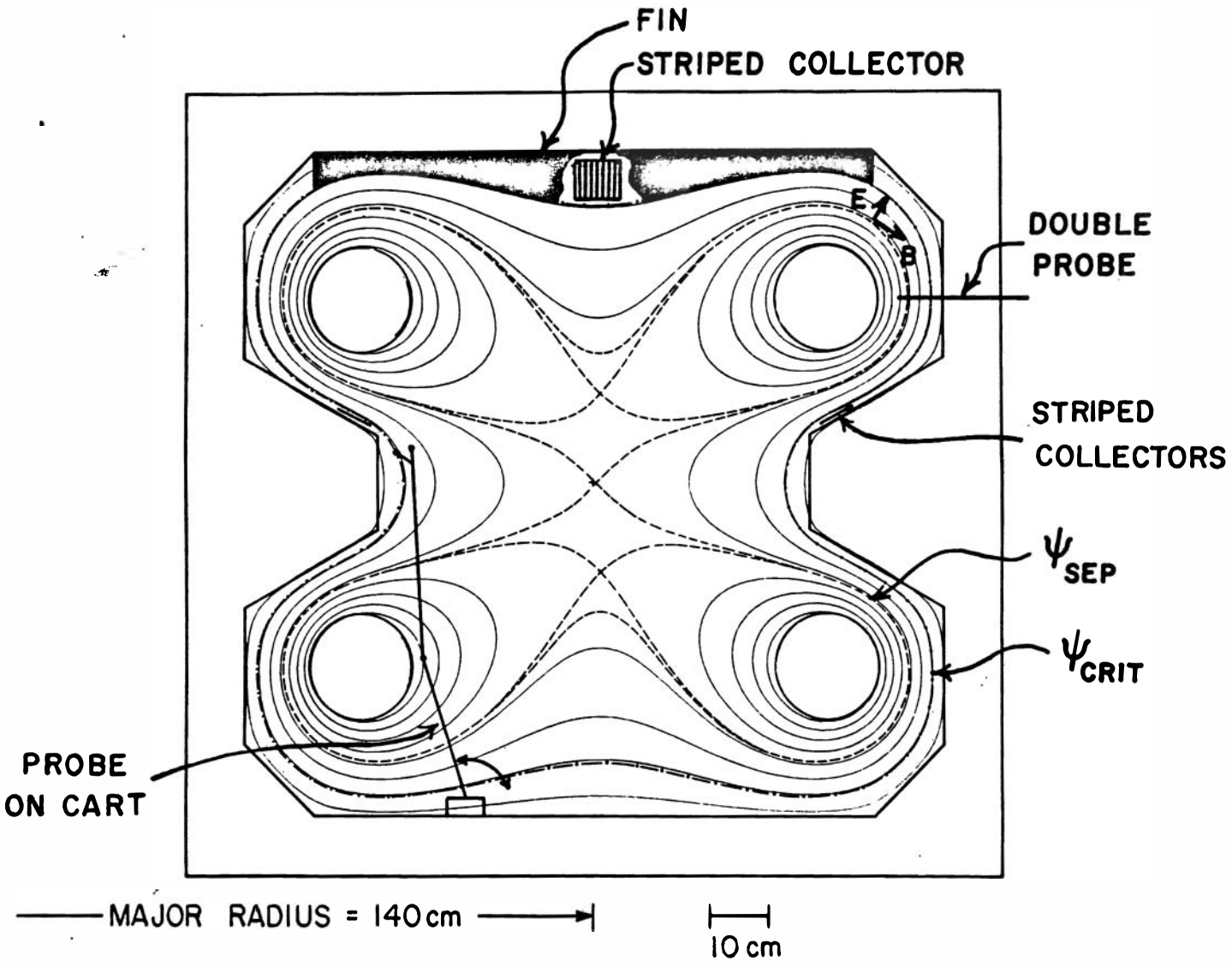
FIN
STRIPED COLLECTOR
E
B
DOUBLE PROBE
STRIPED COLLECTORS
ψ_{SEP}
ψ_{CRIT}
PROBE ON CART
MAJOR RADIUS = 140 cm
10 cm

Figure 2

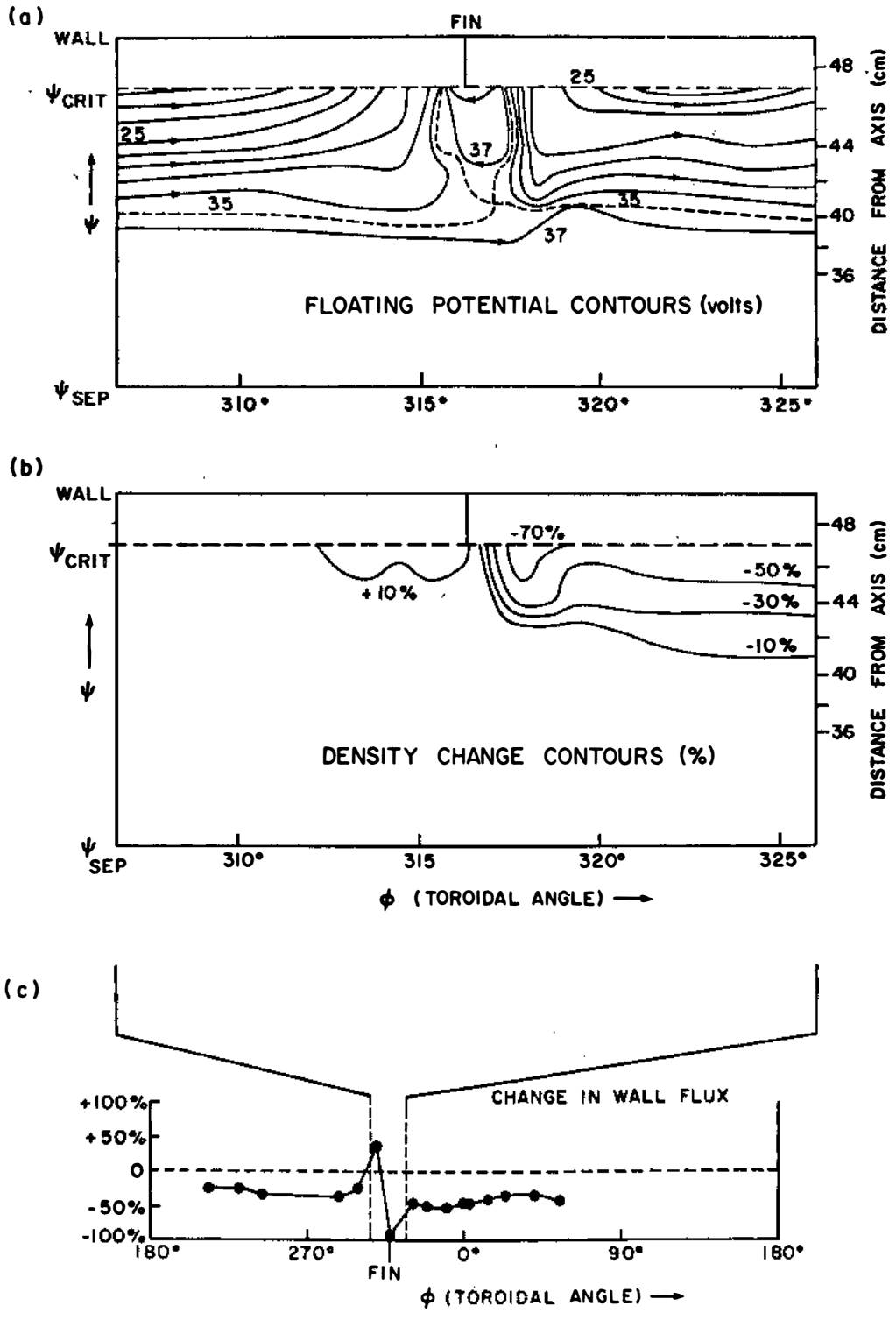
(a)
WALL
FIN
ψ_{CRIT}
25
37
35
ψ_{SEP}
FLOATING POTENTIAL CONTOURS (volts)
310°
315°
320°
325°
48
44
40
36
DISTANCE FROM AXIS (cm)
(b)
WALL
ψ_{CRIT}
-70%
-50%
-30%
-10%
+10%
ψ_{SEP}
DENSITY CHANGE CONTOURS (%)
310°
315
320°
325°
ϕ (TOROIDAL ANGLE) ⟶
48
44
40
36
DISTANCE FROM AXIS (cm)
(c)
CHANGE IN WALL FLUX
+100%
+50%
0
-50%
-100%
180°
270°
FIN
0°
90°
180°
ϕ (TOROIDAL ANGLE) ⟶

Figure 3

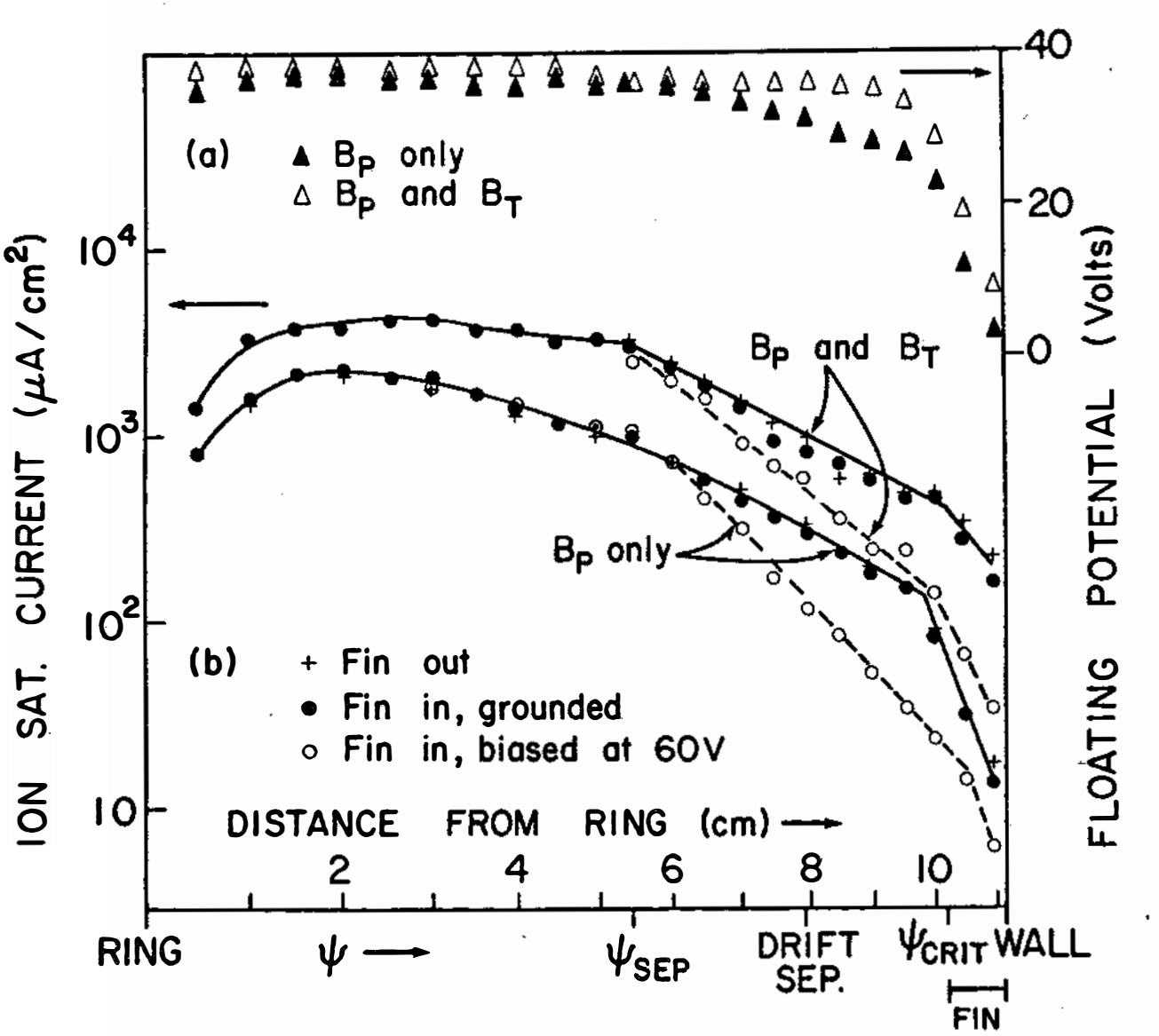
(a) ▲ B_P only
△ B_P and B_T
B_P and B_T
B_P only
(b) + Fin out
● Fin in, grounded
○ Fin in, biased at 60V
ION SAT. CURRENT (μA/cm^2)
FLOATING POTENTIAL (Volts)
10^4
10^3
10^2
10
40
20
0
DISTANCE FROM RING (cm) →
2
4
6
8
10
RING
ψ →
ψ_{SEP}
DRIFT SEP.
ψ_{CRIT}
WALL
FIN

Figure 4